Nuclear Engineering and Technology xxx (xxxx) xxx

Contents lists available at ScienceDirect

Nuclear Engineering and Technology

journal homepage: www.elsevier.com/locate/net

Original Article

Mitigation of seismic responses of actual nuclear piping by a newly developed tuned mass damper device

Shinyoung Kwag [a], Seunghyun Eem [b, *], Jinsung Kwak [c], Hwanho Lee [c], Jinho Oh [c], Gyeong-Hoi Koo [c]

[a] Department of Civil and Environmental Engineering, Hanbat National University, Daejeon, 34158, Republic of Korea
[b] Department of Conversion & Fusion System Engineering, Major in Plant System Engineering, Kyungpook National University, Sangju, Republic of Korea
[c] Korea Atomic Energy Research Institute, 111 Daedeok-daero, Yuseong-gu, Daejeon, 34057, Republic of Korea

a r t i c l e i n f o

Article history:
Received 5 November 2020
Received in revised form
7 February 2021
Accepted 9 February 2021
Available online xxx

Keywords:
Piping
Tuned mass damper (TMD) device
Dynamic absorber
Nuclear power plant
Device design
Device fabrication
Operation test

a b s t r a c t

The purpose of this study is to reduce seismic responses of an actual nuclear piping system using a tuned mass damper (TMD) device. A numerical piping model was developed and validated based on shaking table test results with actual nuclear piping. A TMD for nuclear piping was newly devised in this work. A TMD shape design suitable for nuclear piping systems was conducted, and its operating performance was verified after manufacturing. The response reduction performance of the developed TMD under earthquake loading on actual piping was investigated. Results confirmed that, on average, seismic response reduction rates of 34% in the maximum acceleration response, 41% in the root mean square acceleration response, and 57% in the spectral acceleration response were shown through the TMD application. This developed TMD operated successfully within the seismic response reduction rate of existing TMD optimum design values. Therefore, the developed TMD and dynamic interpretation help improve the nuclear piping's seismic performance.

1. Introduction

Nuclear power plants (NPPs) are comprised of multiple cooling piping systems. A primary cooling system dissipates heat energy generated from nuclear fission. After that, the primary system's heat energy is transferred to turbines through a steam generator to produce electric power. The remaining residual heat is transferred to the secondary and tertiary cooling systems. Because of these multiple interconnected piping systems, a failure in one can induce core damage, and severe damage can lead to radiation leakage and diffusion accidents [1]. Therefore, the safe design, manufacture, and installation of piping are required.

Strong earthquakes have occurred around NPPs, recently. For example, the 2011 East Japan earthquake took place near the Fukushima NPP site, damaging units 1 to 4 and resulting in a radiation leak. In Korea, the 2016 Gyeongju earthquake and the 2017 Pohang earthquake occurred near Wolseong and Gori NPPs. In particular, the 2016 Gyeongju earthquake exceeded the NPP operating-basis earthquake limit, and Wolseong NPP was manually stopped [2]. Thus, accurate evaluation and enhancement of the seismic safety of NPPs are required [3,41]. In particular, improvement of the seismic performance of critical piping systems is one of the highest priorities.

There are two major types of studies on the seismic performance of piping systems. The first is seismic fragility analysis, to evaluate the seismic performance of piping systems. Piping system failures mainly occur at the connections. In particular, it was experimentally found that failure occurred in a tee joint and elbow during seismic loading [4,5]. Thus, research was conducted to investigate the seismic response behavior of the overall piping system, including several connections [6e8]. The dynamic load testing on tee joints and elbows has also revealed their limit states [9,10]. Some studies conducted probabilistic seismic safety analysis of piping systems, considering uncertainties of earthquake ground motions and models [11e13,42].

The second type is studies to improve piping seismic performance. There are three primary lines of research: (1) adding supports and increasing pipe cross-sections; (2) dissipating the input seismic energy by applying a damper-type support device; and (3)

* Corresponding author.
E-mail address: eemsh@knu.ac.kr (S. Eem).

https://doi.org/10.1016/j.net.2021.02.009

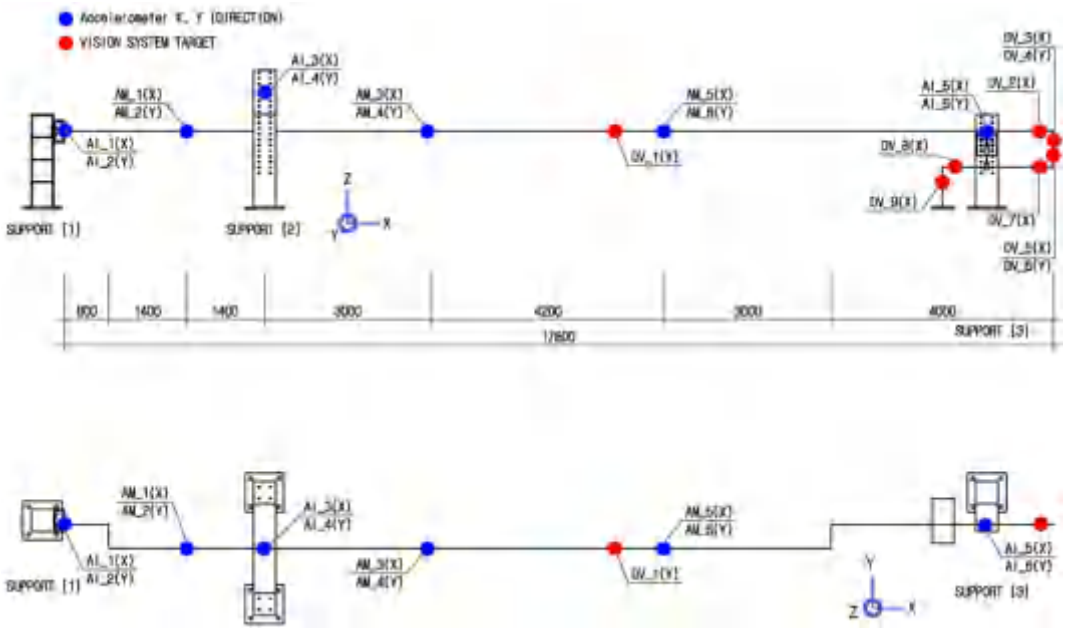

Fig. 1. Schematic design of the test piping.

Fig. 2. The actual configuration of the test piping.

utilizing a tuned mass damper (TMD). Specifically, Kunieda et al. [14] proved theoretically and experimentally that damping devices such as direct dampers, dynamic absorbers, and connected dampers were useful for improving the seismic performance of piping. Park et al. [15] analyzed the effect of a snubber and energy absorption supports on the seismic response of piping by performing shaking table tests and numerical analyses. Fujita et al. [16] analyzed the effect of a nonlinear support device on the seismic response of a piping system. Bakre et al. [17,18] studied the effects of applying sliding friction dampers and x-plate dampers to a piping system based on a shaking table test and numerical analyses. Kumar et al. [19,20] applied a quasi-active variable stiffness damper and passive devices to piping systems and analyzed piping responses to three-way seismic motion inputs.

Until recently, TMDs have been used only for mitigating the constant vibration of piping during normal operation conditions [21]. Song et al. [22], Jiang et al. [23], Wang et al. [24], and Tan et al. [25] experimentally investigated the effect of piping dynamic vibration reduction with a TMD during normal operating conditions. It was recently found that the use of multiple TMDs could reduce the seismic response of a piping system [26].

The TMD has been applied in many fields since Frahm [27] invented the concept. In particular, it was known to effectively control structural responses subjected to dynamic loads, such as

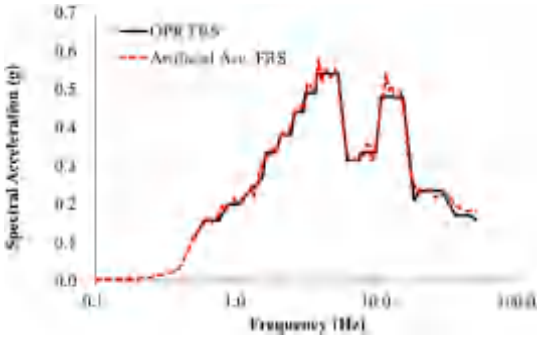

Fig. 3. 5%-damping OPR OBE FRS and the FRS generated from artificial time history acceleration.

wind loads in which a specific frequency was dominant [28]. It was also valid for controlling responses of building structures in earthquake loading [29]. Thus, TMDs are frequently used to reduce the earthquake responses of buildings and civil structures. Recently, studies on reducing earthquake responses of equipment and piping in NPPs through TMDs have been widely conducted [26,30e32].

Studies to date about TMDs for improving piping seismic performance have been focused on numerical aspects [33,43]. However, there are few studies on developing the actual TMD device. Existing TMD devices for decreasing piping vibration during normal operating conditions have not been verified as applicable and effective in reducing the seismic responses of actual NPP piping [22,25]. Therefore, this study proposes a TMD shape design

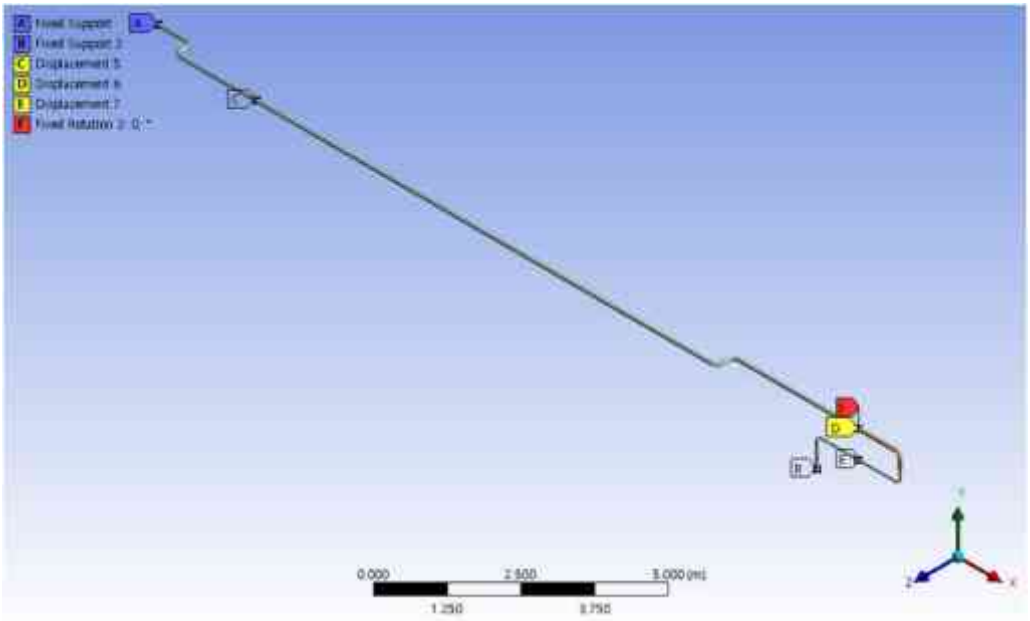

Fig. 4. Numerical piping model.

Table 1
Specifications of the pipe sections.

Nominal Pipe Size	Outside diameter	Inside diameter	Thickness
50.8 mm (2 in)	60.3 mm	42.8 mm	8.74 mm
76.2 mm (3 in)	88.9 mm	66.6 mm	11.13 mm

Table 2
Material properties of the piping system.

Mass density		Young's modulus	Tensile yield strength	Poisson's ratio	Material damping
Stainless Steel	Water				
7954 kg/m^3	1000 kg/m^3	199 GPa	231 MPa	0.3	4.0%

Table 3
Comparison of the natural frequency and the damping ratio for the test and the numerical model.

Component		Mode (#) & Resonant Frequency (Hz)				Damping (%)
		1	2	3	4	
Experiment		1.96	2.23	3.70	6.69	3.56
Analysis	ANSYS	2.02	2.11	3.52	5.68	4.00
	MIDAS	2.02	2.10	3.52	5.67	4.00

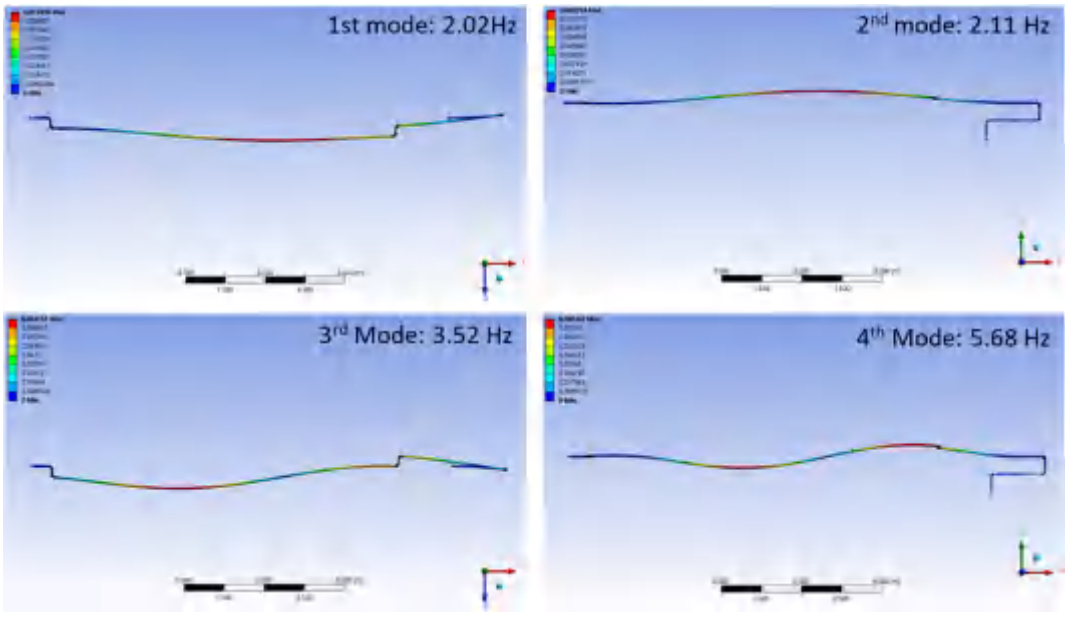

Fig. 5. Mode shapes of the numerical piping model.

Table 4
Mode analysis results of the numerical piping model.

Mode (#)	Frequency (Hz)	X-dir.		Y-dir.		Z-dir.	
		Mass (kg)	Ratio	Mass (kg)	Ratio	Mass (kg)	Ratio
1	2.02	0.32	6.2E-04	0.27	5.4E-04	277.00	0.55
2	2.11	3.3E-04	6.6E-07	253.29	0.50	0.39	7.7E-04
3	3.52	1.75	3.5E-03	2.3E-03	4.6E-06	9.56	0.02
4	5.68	0.00	6.3E-06	0.41	8.2E-04	0.05	9.7E-05
5	7.18	5.76	0.01	0.01	1.4E-05	27.21	0.05
6	11.21	1.9E-05	3.8E-08	39.72	0.08	0.01	2.3E-05
7	13.93	1.21	2.4E-03	0.71	1.4E-03	56.20	0.11
8	15.28	7.11	0.01	0.23	4.6E-04	0.27	5.4E-04
9	18.07	32.52	0.06	1.04	2.0E-03	4.78	0.01
10	19.24	21.42	0.04	0.08	1.7E-04	16.95	0.03
«	«	«	«	«	«	«	«
Total		506.98	1.0	506.98	1.0	506.98	1.0

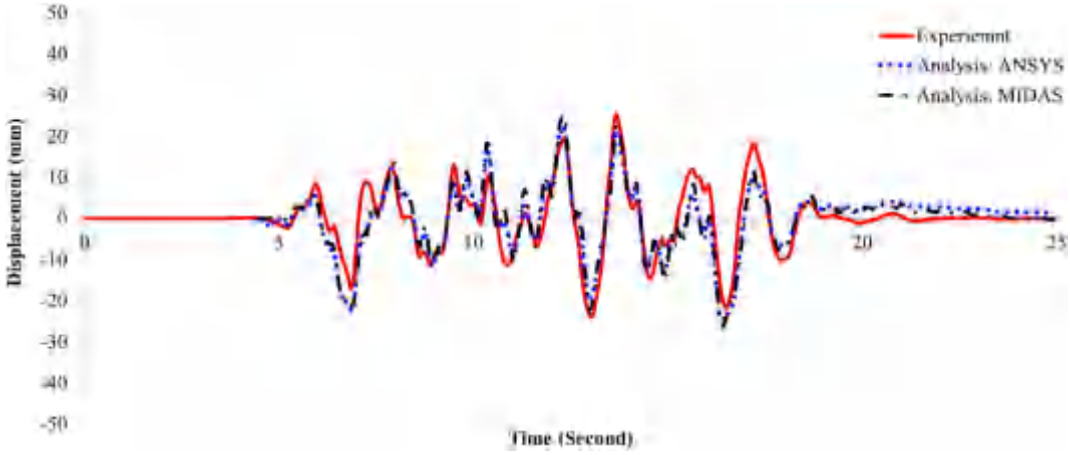

Fig. 6. Comparison of the displacement results at DV3 obtained from the test and the numerical analysis.

Table 5
Optimal TMD design variable equations and methods.

	Optimal TMD design variable equations and methods
Den Hartog [35]	$f_{opt} = \frac{1}{1+m}$ $z_{opt} = \sqrt{\frac{3m}{8(1+m)}}$
Warburton [36]	$f_{opt} = \frac{\sqrt{1-m/2}}{1+m}$ $z_{d_{opt}} = \sqrt{\frac{m(1-m/4)}{4(1+m)(1-m/2)}}$
Sadek et al. [37]	$f_{opt} = \frac{1}{1+m}\left(1 - z\sqrt{\frac{m}{1+m}}\right)$ $z_{d_{opt}} = \frac{z}{1+m} + \sqrt{\frac{m}{1+m}}$
Rana & Soong [38]	Numerical Optimization
Kwag et al. [26]	Numerical Optimization

*m is the mass ratio of TMD mass and the control modal mass.

applicable to NPP piping systems to improve seismic performance. This work also verifies the design, manufacturing, and operation of the TMD device. Finally, this work analyzes the piping seismic response reduction effect through the developed TMD.

Specifically, a numerical model is developed and validated for the actual NPP piping based on shaking table test results. The TMD installation location is determined based on the dynamic characteristics of the validated model. Optimal TMD design values are obtained from the existing optimal design formulas or methods through numerical analyses. A TMD shape design suitable for NPP piping is developed based on the optimal TMD design value range. The developed TMD device is designed with a detachable mass body. Thus, the natural frequency of the TMD can be easily adjusted according to the state of the actual NPP piping site. Next, the TMD device is manufactured, and its operating performance is tested. The fundamental frequency and damping ratio for the TMD device are experimentally identified through free vibration testing. Finally, seismic response mitigation effects are analyzed by applying TMD stiffness and damping values, for which the operating performance has been verified, to a validated numerical piping model.

2. Development and verification of a numerical model for nuclear piping

The Korea Atomic Energy Research Institute (KAERI) and Pusan National University have performed shaking table tests on NPP piping systems [34]. The tested piping system is used at the OPR (Optimized Power Reactor)-1000-type Shin-Kori unit 2. It is a connecting duct when an emergency shut-off of the main piping in the steam turbine is needed. It is installed over two floors of different heights within the containment building. The shaking table test model was 17.8 m long in the longitudinal direction. It consisted of two shaking tables, three frames, supports, connections, and two-inch and three-inch stainless steel pipes with seven elbows and one reducer. The ends of the piping system were

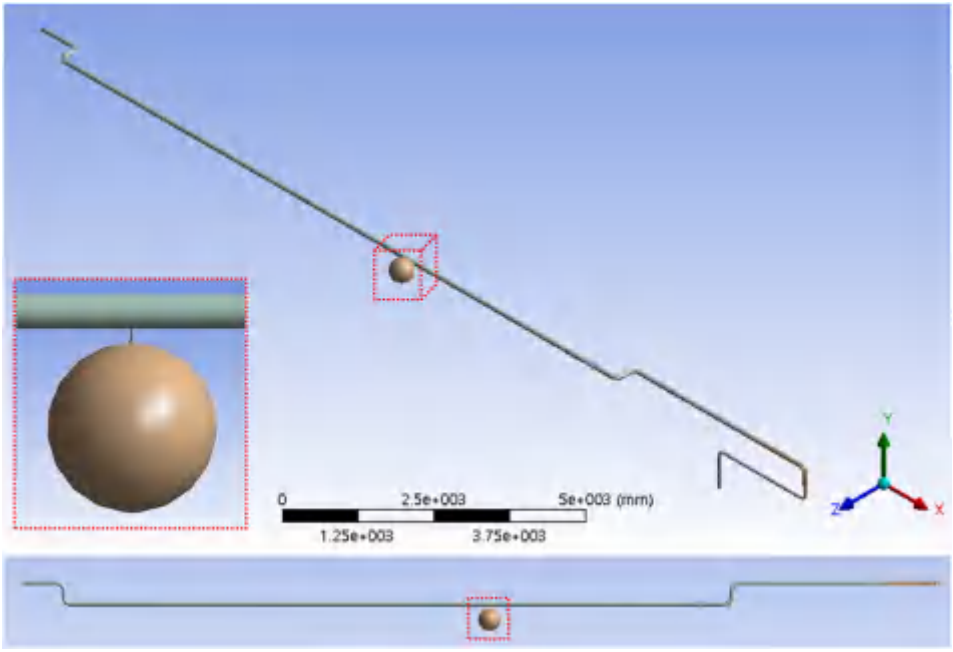

Fig. 7. The TMD installation location in the numerical piping model.

Table 6
Properties of TMD design variables using optimal equations and methods.

Parameters	Den Hartog	Warburton	Sadek et al.	Rana & Soong	Kwag et al.
Mass (kg)	16				
Mass ratio (m)	0.058				
Optimal frequency ratio (f_{opt})	0.945	0.932	0.937	0.925	0.960
Optimal damping ratio (z_{opt})	0.143	0.118	0.271	0.152	0.148
Stiffness (N/m)	2304	2237	2261	2206	2375
Damping (N·s/m)	55	45	103	58	58

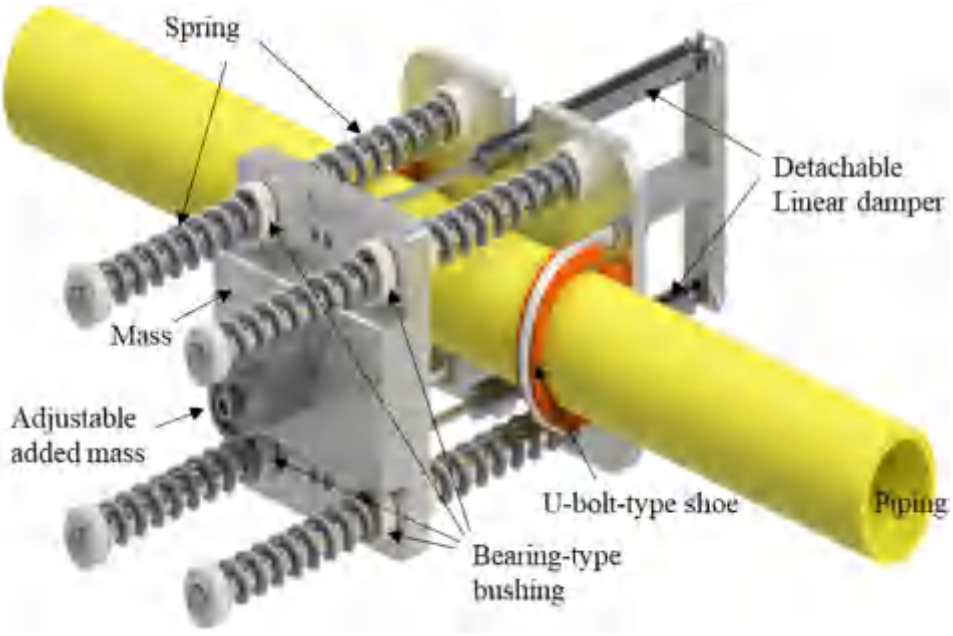

Fig. 8. Design of the TMD device.

installed on different shaking tables. Two frames were installed on the left shaking table, and the other was installed on the right shaking table. A fixed end connection, hanger support, and simple support were set up using these frames. The schematic design and overall piping configuration are represented in Fig. 1 and Fig. 2, respectively. The input earthquake ground motion used was an artificial ground motion enveloping the operating-basis earthquake (OBE) floor response spectrum (FRS) applied to the containment wall of an NPP of about 33.83 m (111 ft) in height (see Fig. 3). As a rough test result, the measured natural frequencies were revealed for the first mode at 1.96 Hz, the second mode at 2.23 Hz, the third mode at 3.70 Hz, and the fourth mode at 6.69 Hz through Fast Fourier Transform (FFT) analysis of the measured response. The measured damping ratio was estimated to be 3.56% by the logarithmic decrement damping formula from the free vibration response signals. Other significant data concerning the piping responses are detailed in the KAERI report [34].

Based on the shaking table test results in this study, a finite element numerical model of the piping was created. ANSYS and MIDAS GEN were used for numerical analysis. When establishing the analysis model, the beam element was applied as the piping element. Additional masses were applied to consider the inertial force of water inside the piping. The specific boundary conditions and shape are shown in Fig. 4. The dimensions of pipe sections are summarized in Table 1, and the related material properties are listed in Table 2. The numerical analysis was performed by seismic response analysis based on the time history, and the damping matrix in the time history analysis was generated using the Rayleigh damping approach. For the natural frequency and the damping ratio, Table 3 compares the measurement results obtained from the piping shaking table test and the calculated values from the numerical analysis. It can be seen that the natural frequency and the damping ratio results of the test and the numerical analysis are similar. Fig. 5 and Table 4 show the mode shapes related to the natural frequencies of the piping system. Fig. 6 shows the measured displacement at the position between the elbow and the reducer (i.e., DV3) and time history analysis results at the same position under the seismic input motion of the OBE FRS of Fig. 3 (Y-Direction in Fig. 1 and Z-Direction in Fig. 4). Fig. 6 compares the displacement results at point DV3 from the measurement and the analysis in the time-series domain. As shown in Fig. 6, the seismic displacement response results of the shaking table test and the numerical analysis are similar in terms of the response period, waveform, and amplitude. Slight deviations in the test results and numerical analysis come from the friction characteristics of the piping supports, uncertainty in the material properties, and piping geometrical dimensions.

3. Optimal TMD design for nuclear piping

Den Hartog [35] proposed the closed-form TMD design equations for optimal frequency ratio (f_{opt}) and optimal damping ratio (z_{opt}). Such equations were derived by minimizing the steady-state response of a structure subjected to harmonic excitation acting on

Table 7
The design variable values and test results of the TMD spring.

Items	Values
Shear stiffness (G)	78 GPa
Spring wire diameter (d)	2.6 mm
Inner diameter of the spring coil (D_1)	32 mm
Effective number of turns (N)	37 turns
Effective stiffness (K_{eff})	290.7 N/m (Total 8 EA: 2325.6 N/m)
Target range of effective stiffness (From Table 6)	275.8e296.9 N/m (Total 8 EA: 2206e2375 N/m)
Average test result	301.5 N/m (Total 8 EA: 2412 N/m)

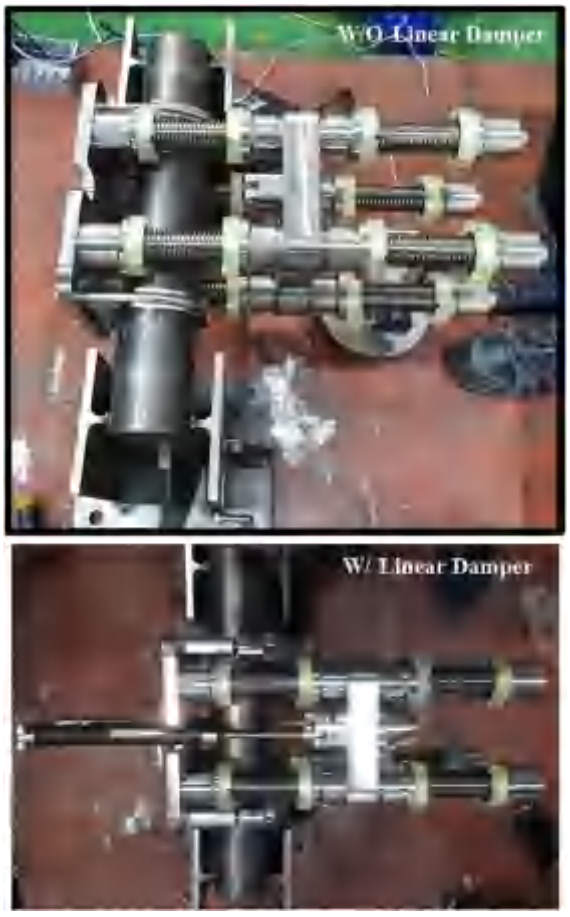

Fig. 9. The manufactured TMD installed in the piping jig.

the structure's mass. Warburton [36] presented the optimal design equations of a TMD for structures subject to random ground acceleration in the form of white noise. The inherent damping of the structure was not considered in deriving the above optimal TMD design equations. Accordingly, Sadek et al. [37] proposed optimal design equations of a TMD for structures subjected to earthquake loads, considering the damping of the structure. Rana and Soong [38] proposed a method to derive the optimal TMD design variables' values through numerical optimization. They targeted a structure subjected to earthquake loads and considered the damping of the structure while finding the optimal design variables. However, their study did not take into account the combined effects of several modes because the TMD-mounted multi-degrees-of-freedom (DOF) structure was simplified to a two-DOF structure during a numerical optimization. Hence, recently, Kwag et al. [26] proposed a method for finding optimal design variables for TMDs in a multi-DOF piping system with multiple TMDs subjected to earthquake loads. The optimal TMD design formulas and methods mentioned above are summarized in Table 5.

Installing TMDs for all modes can significantly reduce the target piping seismic responses. There are some cases, however, for which it is not possible to install TMDs. These include, but are not limited to, installation space restrictions, changes in the piping system's dynamic characteristics, and economic costs. Also, the use of TMDs in some locations is ineffective, depending on the mass of the control mode or the input seismic spectrum's shape. This study installed one TMD at a single location. The optimal TMD design was performed for a one-directional horizontal seismic load (Z-direction of the model). According to the modal analysis results (see Table 4), the first mode contributed the most to the overall response of the direction considered. Thus, the TMD was installed at the location where the first mode's most considerable deformation occurs. The TMD mass was set as 16 kg because this value did not change the dynamic characteristics and stress state. The mass ratio of the TMD mass and the control modal mass (1st effective modal mass: 277 kg) is calculated as $\mu = 0.058$. The numerical piping model with the TMD attached is shown in Fig. 7. The detailed TMD design variable values obtained from the optimal TMD design formulas and methods are summarized in Table 6.

4. Shape design, fabrication, and operation performance test of the TMD

Even if the optimal design variable values are obtained for an actual TMD device, it is difficult to accurately implement such a design due to realistic limitations in the fabrication of the actual shape. For example, the diameter of a spring steel wire can be manufactured only in integer units. In the case of a damping device, it is difficult to predict an accurate damping ratio in advance. Specifically, a bushing used as a damping device implements an energy dissipation by a frictional force, and in this case, the damping ratio can be accurately predicted only by measuring through an experiment.

The spring and damping devices that were implemented were selected based on the optimal TMD design value range derived in Section 3. The detailed shape of the TMD to be attached to the existing piping system was devised, as shown in Fig. 8. The TMD and the piping are combined using a U-bolt shoe. The mass of the TMD is arranged as close as possible to the cross-section of the piping. Springs are arranged on both sides of the mass body of the TMD. It is also possible to attach and detach an additional mass so that the TMD frequency can be adjusted finely according to the site situation. This is because one factor that can determine the frequency ratio of the TMD is the mass. The other factor is spring stiffness, but stiffness change is not easy after its fabrication and once the installation is complete. The damping device attaches as bearing-type bushings arranged at the corners of the mass body to dissipate friction energy. Furthermore, detachable linear dampers can be implemented opposite the mass body when an additional damping device is needed. The damping device is implemented this way because the damping ratio due to friction is not easy to predict. If needed, a damping force can be added through the auxiliary device. For ease of maintenance, the fastening portions of the main components are on the outside.

In this study, the TMD mass was selected as a default value of 16 kg and configured to allow correction in the range of 14e19 kg. This feature enables finely adjusting the TMD frequency by adding or subtracting a correction mass through measurement after installation in the field. The stiffness of the spring is determined using the material shear stiffness (G), the spring wire diameter (d), the inner diameter of the spring coil (D_1), and the effective number of turns (N) by the following equation [39].

$$K_{eff} = G\$\frac{D_1^4}{8\$N\$d^3} \quad (1)$$

Because the spring geometry is limited by the possible dimensions of the manufacturing machine, it is virtually impossible to manufacture springs equal to the optimum design value for the TMD's stiffness. Accordingly, the total spring stiffness was selected to have a value within the range of the optimum design stiffness value determined in Table 6. The design variable values for spring stiffness and the related test results of the TMD are summarized in

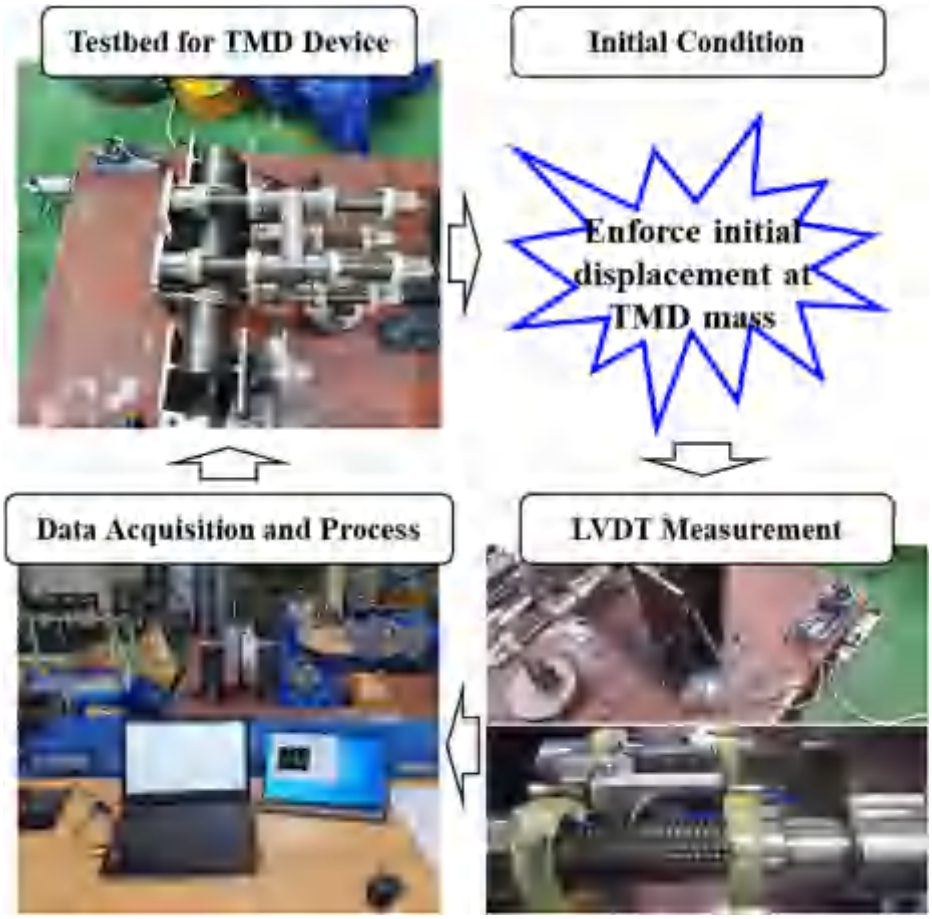

Fig. 10. Schematic procedure for the free vibration test of the TMD device.

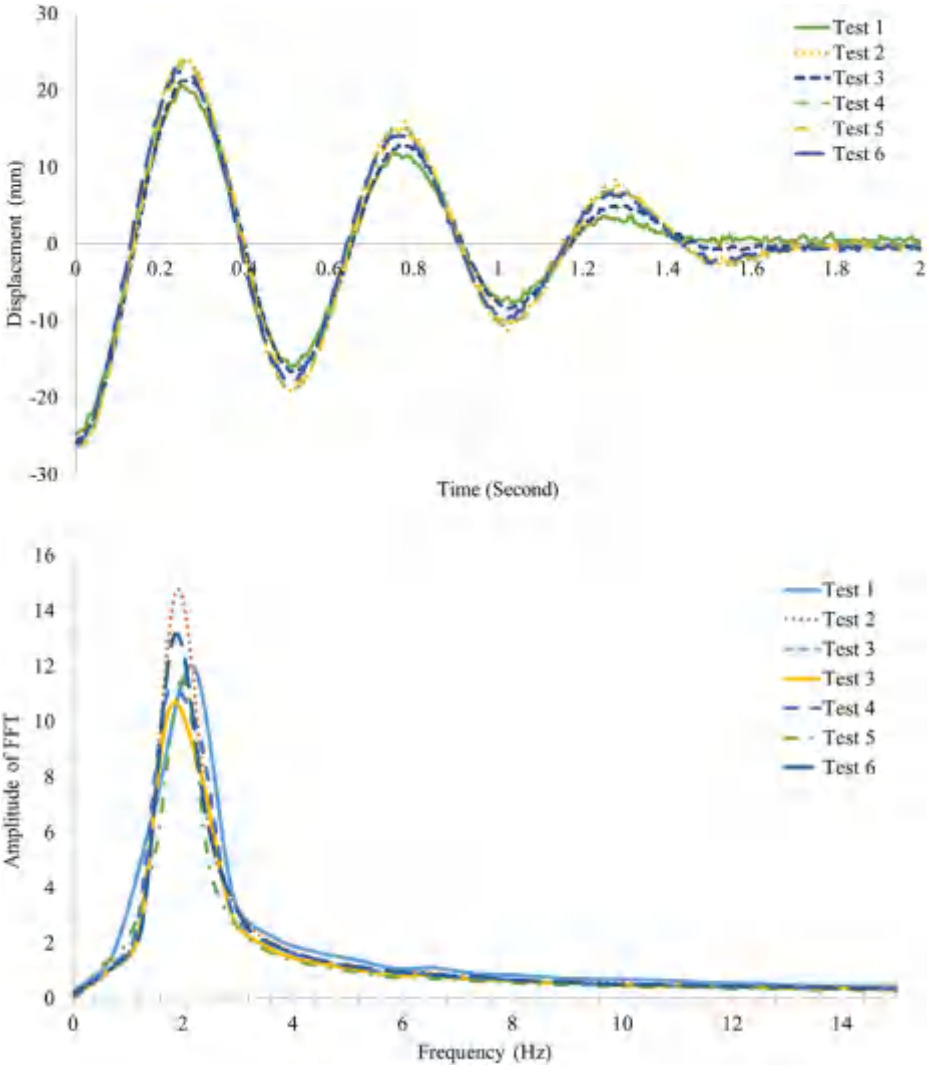

Fig. 11. The time-series data and FFT graph for the free vibration tests of the TMD.

Table 8
Summary of free vibration test results of the manufactured TMD.

Test No.	1	2	3	4	5	6	Avg.
Frequency (Hz)	1.985	1.954	1.969	1.954	1.954	1.954	1.962
Damping ratio	0.148	0.080	0.120	0.094	0.093	0.096	0.105

Table 7. Four damping devices are implemented at the corners of the mass body as bearing-type bushings so that the damping force was realized through friction between the ball bearing and the rod guide when a movement of the TMD mass occurred. The springs and damping devices are arranged so that the TMD mass can move within a stroke range of ±90 mm from the neutral state. The TMD stroke was determined by considering interference with other structures and the maximum displacement of the TMD under seismic design load.

Next, a TMD device was fabricated based on the shape design. The final fabricated TMD is shown in Fig. 9, with and without a linear damper as an additional damping device. A free vibration test was performed on the TMD without a linear damper to verify the operating performance and investigate the bushing friction damping ratio. Fig. 10 shows the schematic for the free vibration tests of the TMD device. First, the TMD device was set up in the piping jig of the testbed. The initial displacement was enforced at the TMD mass to perform a free vibration test. The displacement of the moving TMD mass was measured using a linear variable differential transformer (LVDT). The measured displacement response was recorded and post-processed through the data processing system. Such tests were performed six times. Fig. 11 shows the measured time-series data and the FFT graph for these test results. Based on the test results in Fig. 11, the natural frequency (f) and the damping ratio (ζ) of the TMD were obtained using the following equations [40]:

$$f = \frac{1}{T} = \frac{j}{t_{j+m} - t_m} \tag{2}$$

$$\zeta = \frac{1}{2\pi}\frac{1}{j}\ln\left(\frac{u_m}{u_{j+m}}\right) \tag{3}$$

where u_m is an m^{th} cycle peak displacement at time t_m. u_{j+m} is a $(j + m)^{th}$ cycle peak displacement at time t_{j+m}. The calculated results are summarized in Table 8. On average, the fabricated TMD was confirmed to have a natural period of about 1.96 Hz (i.e., the frequency ratio: 0.96) and a damping ratio of about 11%. These

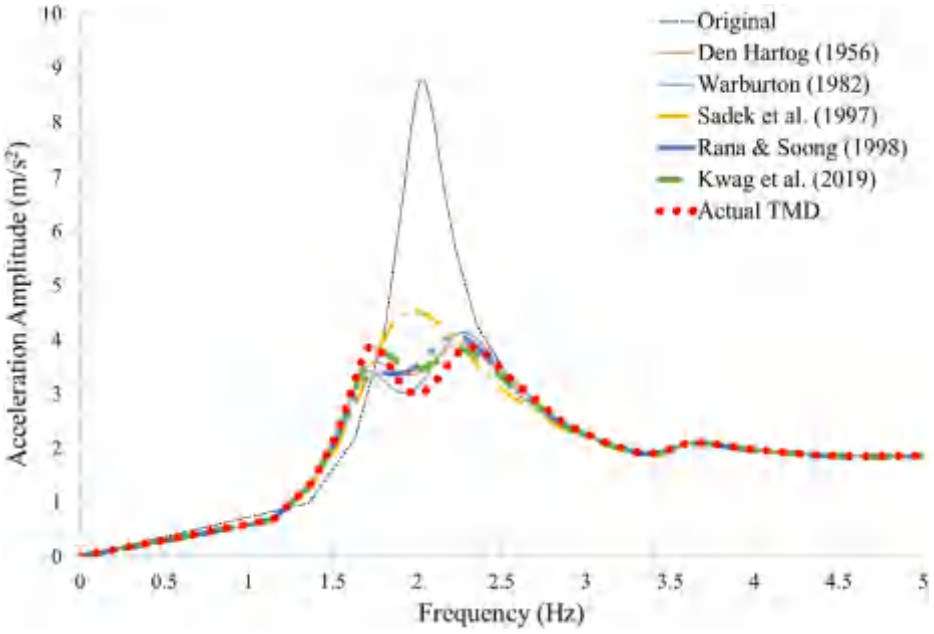

Fig. 12. Comparison of maximum acceleration responses by frequencies at the TMD location in the piping.

Table 9
Mode analysis results for the numerical piping model with the TMD design variable values obtained from the Den Hartog (1956) equation.

Mode (#)	Frequency (Hz)	X-dir.		Y-dir.		Z-dir.	
		Mass (kg)	Ratio	Mass (kg)	Ratio	Mass (kg)	Ratio
1	1.69	0.11	2.19E-04	0.01	1.27E-05	163.80	0.31
2	2.00	7.13E-06	1.36E-08	267.33	0.51	1.20E-03	2.29E-06
3	2.27	0.23	4.46E-04	0.02	4.70E-05	129.37	0.25
4	3.52	1.55	2.96E-03	2.31E-03	4.43E-06	10.08	0.02
5	5.67	3.07E-03	5.88E-06	0.63	1.21E-03	0.05	9.11E-05
6	7.19	6.28	0.01	0.01	2.13E-05	26.91	0.05
7	10.83	3.83E-05	7.33E-08	41.58	0.08	0.09	1.63E-04
8	13.84	0.89	1.71E-03	0.21	4.03E-04	55.80	0.11
9	15.18	9.36	0.02	0.09	1.72E-04	0.52	1.00E-03
10	18.05	34.94	0.07	1.05	2.01E-03	4.76	0.01
«	«	«	«	«	«	«	«
Total		522.98	1.0	522.98	1.0	522.98	1.0

values do not precisely coincide with the optimal TMD design variable values of specific design formulas and methods due to practical constraints. Nevertheless, these are values within the range of results of the design formulas and methods considered. Accordingly, to confirm the functional performance of the TMD device developed in this study, seismic responses are analyzed by applying the TMD, whose operational performance is verified, to the previously validated numerical piping model. The effectiveness of the developed TMD device performance is also verified by a comparison study with the results of TMDs designed through other design formulas and methods.

5. Performance verification of the TMD through numerical analysis

5.1. Frequency response analysis results

To confirm the response reduction effect in the developed TMD device's target frequency range, a harmonic excitation with unit acceleration but different loading frequencies was applied as an input to the piping, with and without the TMD. Piping systems with the TMD have the optimal TMD design variable values obtained from several methods. As a result, the maximum acceleration response diagrams at the TMD installation location were compared according to frequency changes of the input acceleration (refer to Fig. 12). Fig. 12 confirmed that the peak acceleration response of piping with the TMD is reduced by 49%e57% compared to piping without the TMD. Such a phenomenon occurred in the frequency of target piping control mode (i.e., 2.02 Hz) because the TMD offsets the response by distributing the target control mode into two modes. This effect was confirmed by the mode analysis results for piping with and without the TMD (refer to Table 4 for results of piping without the TMD, and Table 9 for those of piping with the TMD). The TMD disperses 277 kg of the target control mode mass (at 2.02 Hz) into about 164 kg (at 1.69 Hz) and 129 kg (at 2.27 Hz), respectively. The TMD designed by Kwag et al. [26] shows the most

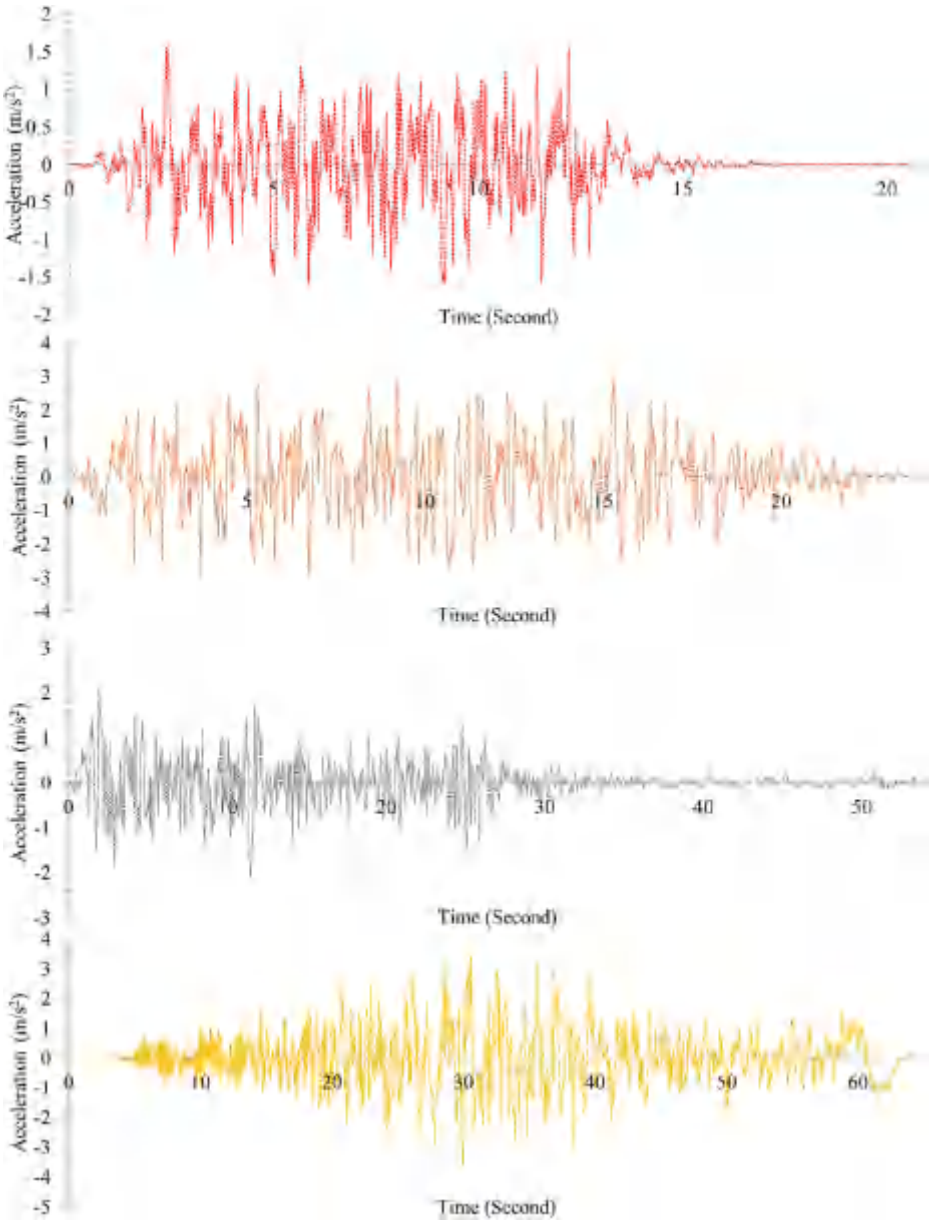

Fig. 13. ATH loading data for input earthquakes.

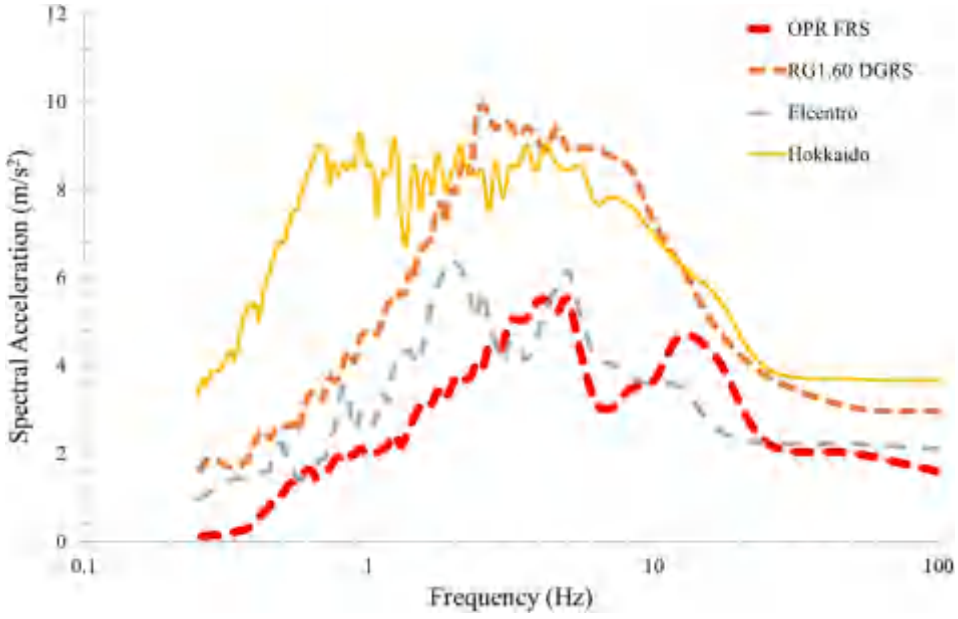

Fig. 14. The 5%-damping seismic response spectra obtained from the input ATHs.

excellent control effect due to the method characteristics. The Sadek et al. [37] shows a relatively small control effect compared to other formulas and methods. The actual designed and manufactured TMD of this study shows a control effect of about 56%.

5.2. Time history analysis results

We investigate how much responses were reduced using the TMD under seismic loading. Four earthquake acceleration time history (ATH) loading data were used to verify the response reduction performance of the piping with the TMD. The ATH loading data are from the piping shaking table test, the design ground response spectrum (DGRS) of USNRC Regulatory Guide 1.60 [44], the 1940 El Centro earthquake, and the 2003 Hokkaido earthquake. Fig. 13 shows the detailed ATH loading data for input earthquakes. Fig. 14 illustrates the 5%-damping seismic response spectra obtained from these ATHs.

Fig. 15a, Fig. 16a, Fig. 17a, and Fig. 18a compare the acceleration responses at the TMD installation location in the piping system in the time domains of the four earthquake loadings. According to the presence or absence of the TMD, the maximum acceleration responses and related response ratios are summarized in Table 10. Here, the response ratio is defined as the piping response with the TMD installed divided by the piping response without the TMD. Accordingly, the smaller the defined response ratio value, the higher the response reduction is. Table 11 summarizes the root mean square (RMS) acceleration response and related response ratio. Figs. 15b, 16b and 17b, and Fig. 18b compare the response spectra calculated from the TMD installation location's acceleration responses. Table 12 summarizes the maximum spectral acceleration responses and related response ratios. Detailed discussions of these results follow.

In Figs. 15a–18a, the reduction rate for the time-series maximum acceleration responses ranged from 27% to 39% according to the earthquake ATH loading data and different optimal TMD design methods. The average response reduction rate ranged from 32% to 36%. The Warbuton's [36] equation and Rana and Soong's [38] method show the most excellent control performance with an average response reduction rate of 36%, while the formula of Sadek et al. [37] shows the lowest control performance with an average response reduction rate of 32%. The actual TMD shows an average response reduction rate of about 34%.

The reduction rate for the time-series RMS acceleration responses ranged from 32% to 50%. The average response reduction rate ranged from 39% to 41%. The equation of [37] shows an average response reduction rate of 39%, while the remaining formulas and methods show an average response reduction rate of 41%. The actual TMD shows an average response reduction rate of about 41%.

Based on Figs. 15b–18b, it can be confirmed that the TMD effectively controls the piping target mode. The response reduction phenomenon in the frequency range of the primary piping mode stands out. The response reduction rate for the maximum spectral acceleration ranged from 36% to 71%. The average response reduction rate ranged from 47% to 55%. The formulas and methods of Den Hartog (1956), Warburton [36], and Kwag et al. [26] show an average response reduction rate of 55% and the most excellent control performance, while the formula of Sadek et al. [37] shows the lowest control performance with a 47% average response reduction. The actual TMD shows an average response reduction rate of about 57%.

The designed TMD is the highest in maximum spectral acceleration response and lowest in the maximum acceleration response in terms of the response reduction rate. Such results can also be confirmed by the acceleration response spectra in Figs. 15b–18b. These show that the response control capability is excellent in the first mode of the piping targeted by the TMD and is relatively degraded in the peak acceleration response (i.e., the tail region of acceleration response spectra) in the high-frequency mode not targeted.

When comparing performances according to the optimal TMD design formulas and methods, there was no significant difference in the performance of the designed TMD and the design formulas and methods except for the formula of Sadek et al. [37]. However, compared to the other formulas and methods, the equation of Sadek et al. [37] is about 4%, 2%, and 8% smaller in the maximum acceleration response reduction rate, the RMS acceleration response, and the maximum spectral acceleration response, respectively. This result indicates that this method shows relatively low performance. This phenomenon may occur because this

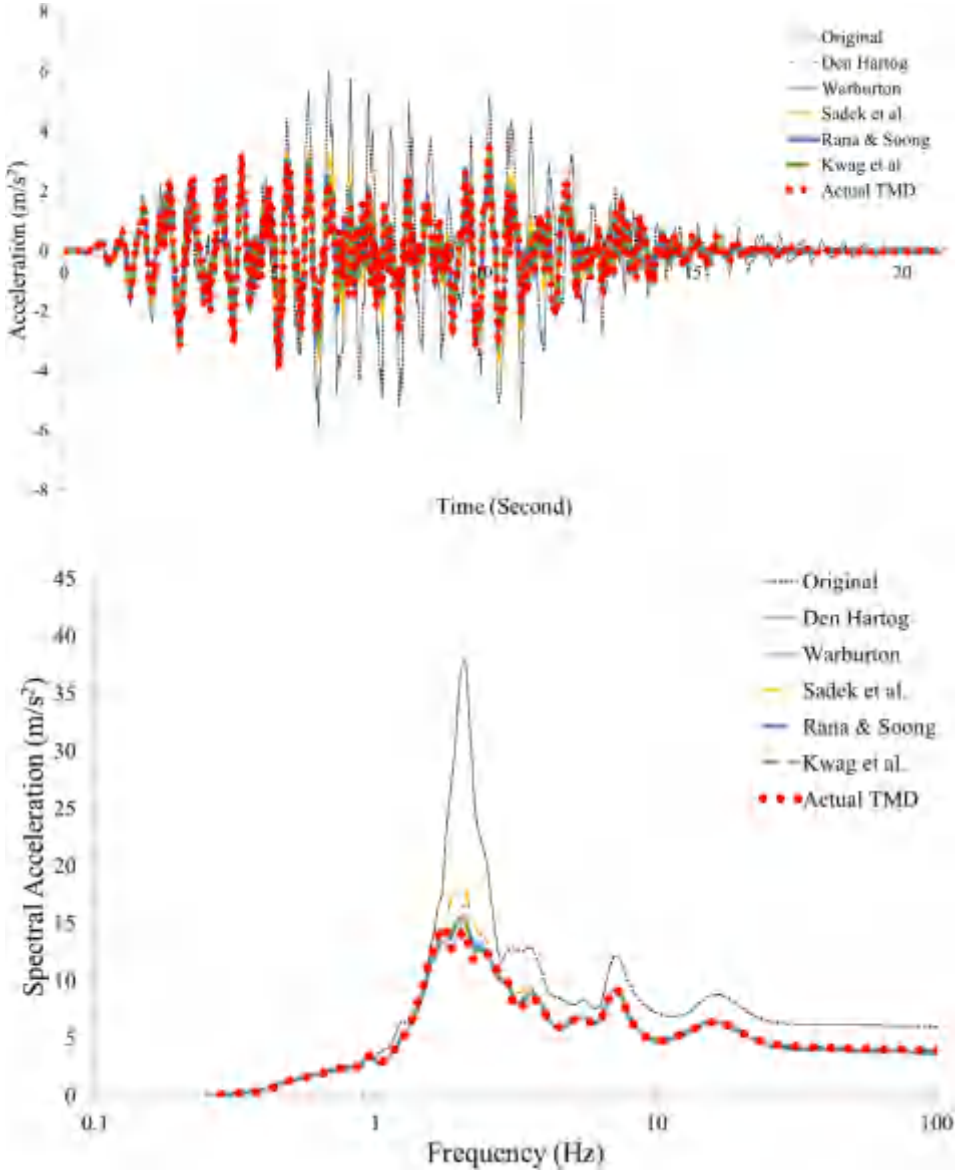

Fig. 15. Responses at the TMD installation location of piping under OPR FRS compatible earthquake loading: (a) time-series acceleration responses (b) response spectra.

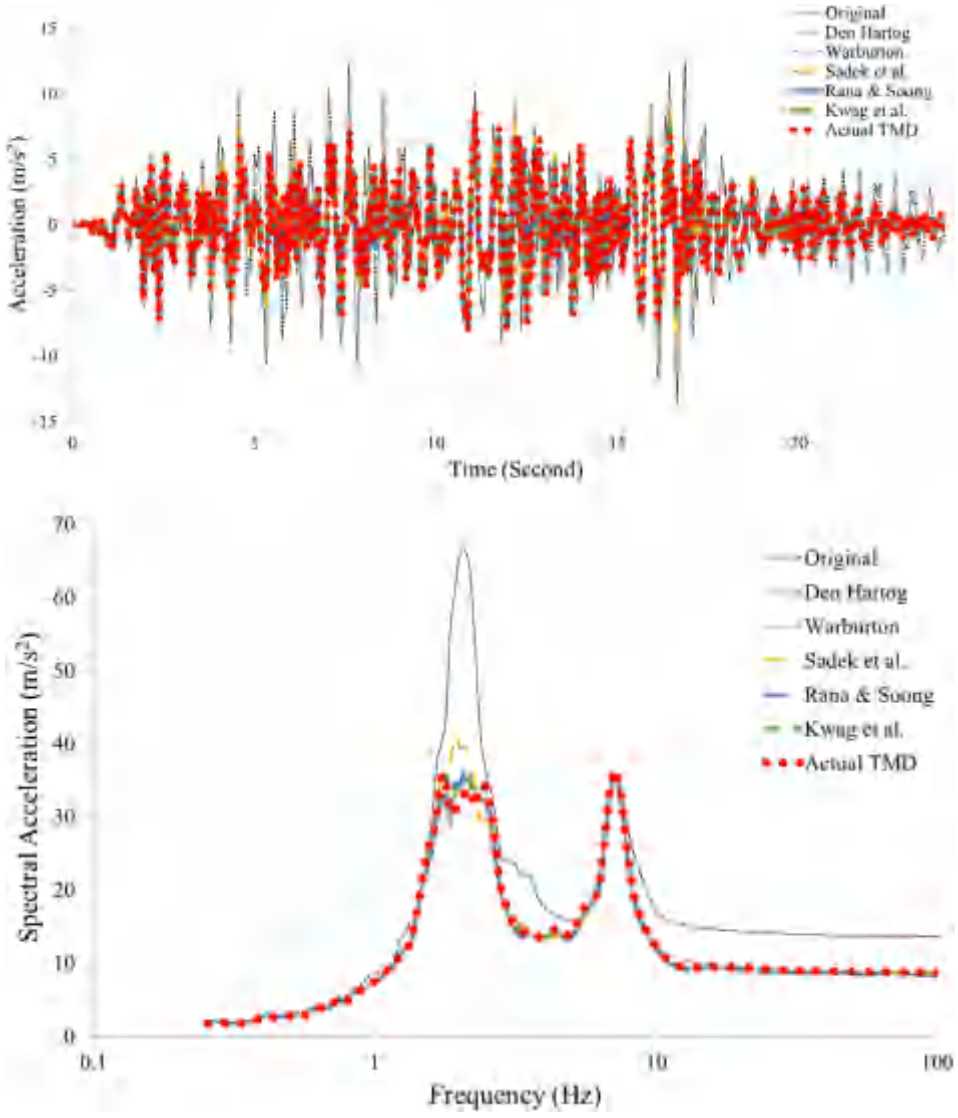

Fig. 16. Responses at the TMD installation location of piping under DGRS compatible earthquake loading: (a) time-series acceleration responses (b) response spectra.

equation uses a TMD with a similar frequency and a relatively large damping ratio compared to other design equations and methods. A TMD with a considerable damping ratio value can dissipate relatively more seismic energy flowing into the TMD, but this can weaken TMD's mobility, thereby reducing the control capability in the target mode.

The TMD fabricated in this study performed well. Its response reduction rates for the maximum acceleration response, the RMS acceleration response, and the maximum spectral acceleration response were within the response reduction rate range of the existing TMD design formulas and design methods. The response reduction rate for the maximum spectral acceleration response of the actual TMD was greater than that of the existing design formulas and methods. Consequently, it is believed that the TMD device developed in this study can be effectively used to reduce earthquake responses of piping and improve seismic performance in actual NPPs.

6. Summary and conclusions

This study analyzed the seismic response reduction effect on an actual NPP piping system using a newly developed TMD device. For this purpose, a numerical piping model was developed and validated based on shaking table test results on the existing nuclear piping. To increase the applicability of the developed TMD to NPP piping at an actual site, we made an additional mass attachable and detachable so the natural frequency of the TMD could be easily adjusted. Also, the TMD device's shape was implemented so that an additional damping device could be easily attached. The optimal TMD design variable values were derived using the existing formulas and methods based on such a design. The TMD operation performance was tested after its fabrication. Finally, the developed TMD's response reduction performance in an existing piping system under earthquake loading was investigated.

Results confirmed that average seismic response reduction rates of 34% in the maximum acceleration response, 41% in the RMS acceleration response, and 57% in the spectral acceleration response with the developed TMD. This TMD operated successfully

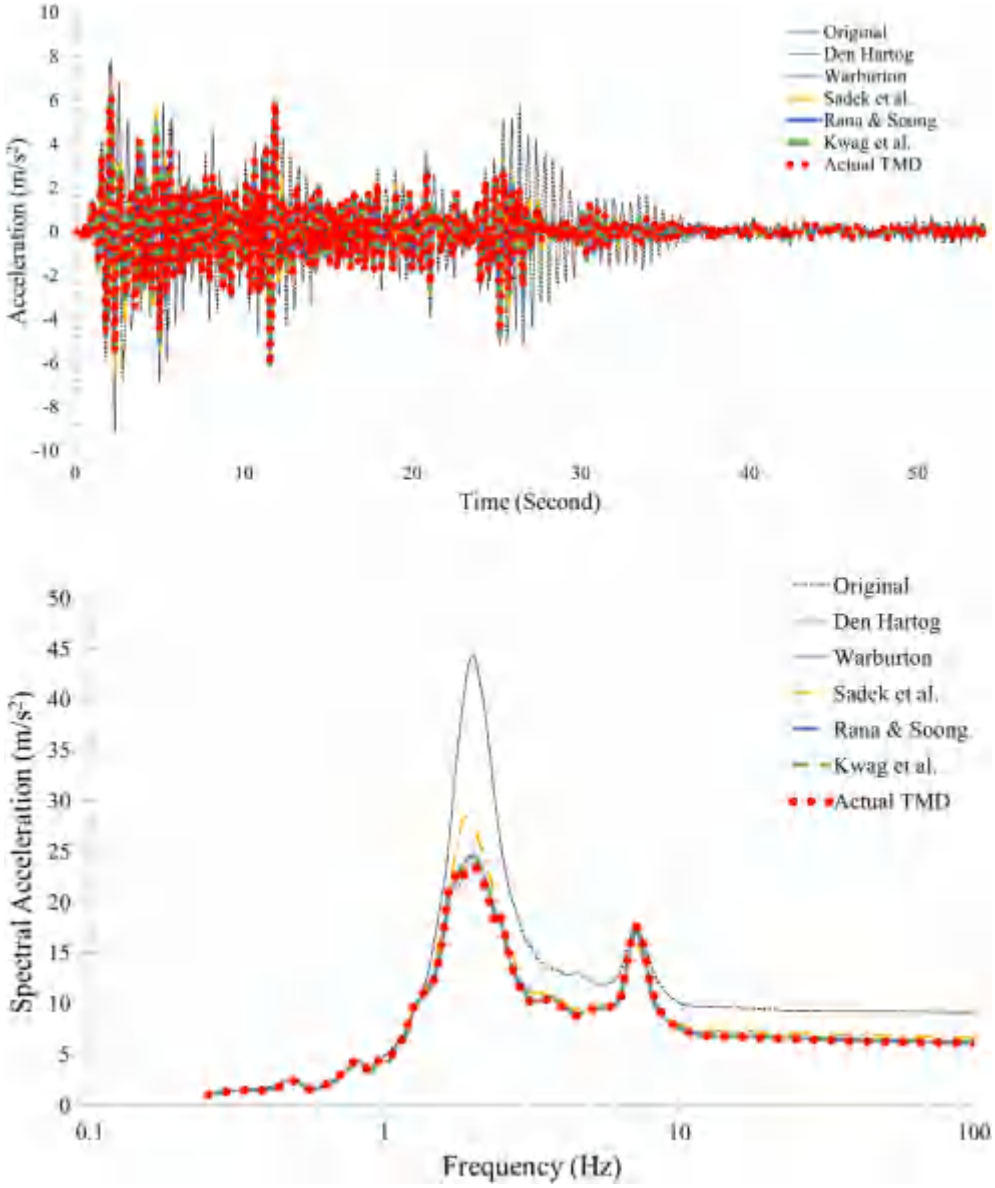

Fig. 17. Responses at the TMD installation location of piping under El Centro earthquake loading: (a) time-series acceleration responses (b) response spectra.

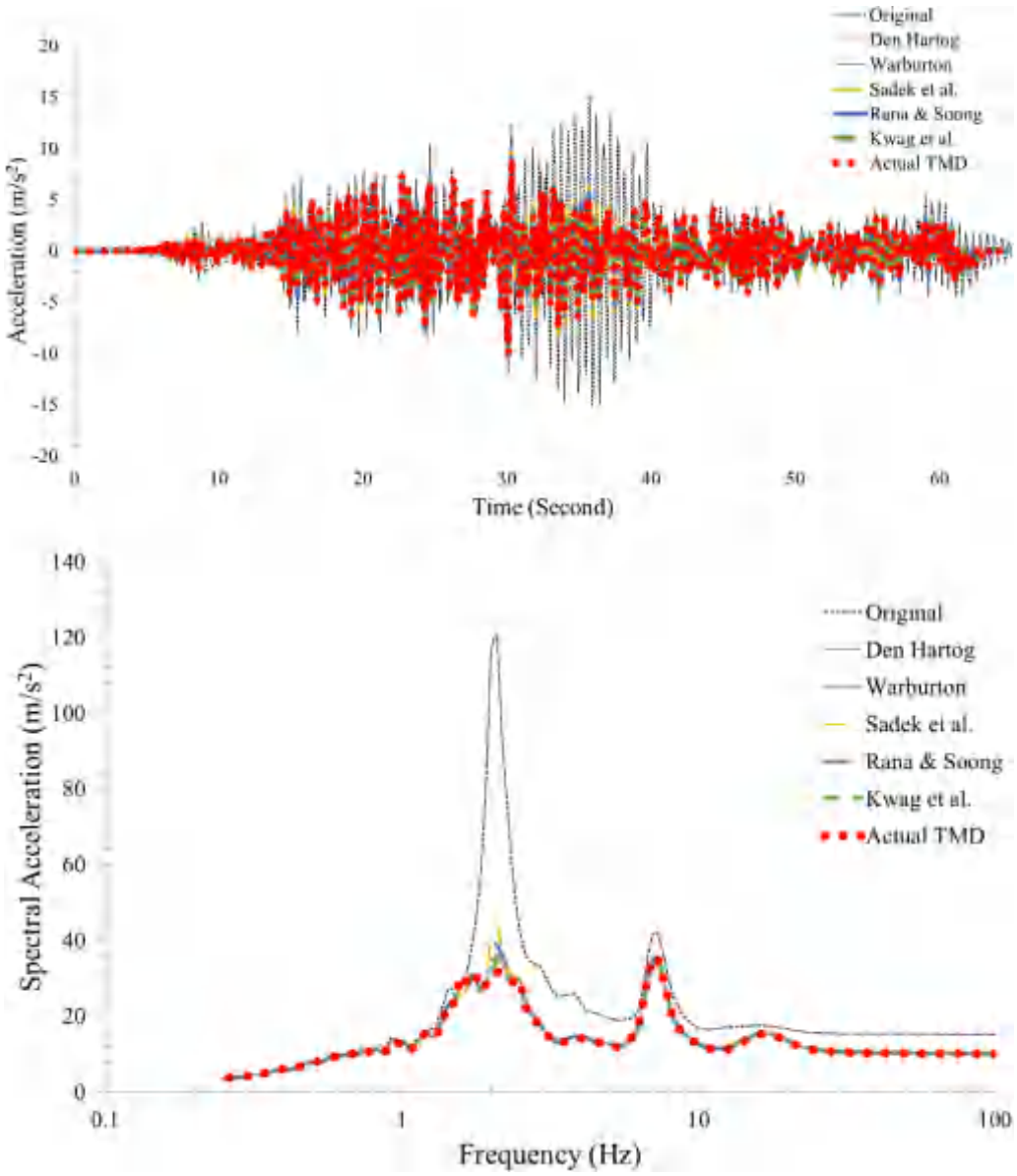

Fig. 18. Responses at the TMD installation location of piping under Hokkaido earthquake loading: (a) time-series acceleration responses (b) response spectra.

Table 10
Comparison of time-series maximum acceleration responses.

Earthquake ground motions	Unit	w/o TMD	w/TMD					
			Den Hartog	Warburton	Sadek et al.	Rana & Soong	Kwag et al.	Actual TMD
OPR FRS	m/s^2	6.03	3.82	3.72	3.81	3.72	3.90	3.96
	Ratio	e	0.63	0.62	0.63	0.62	0.65	0.66
DGRS	m/s^2	13.60	8.47	8.51	8.76	8.36	8.50	8.72
	Ratio	e	0.62	0.63	0.64	0.61	0.63	0.64
El Centro	m/s^2	9.14	6.17	6.01	6.65	6.17	6.22	6.15
	Ratio	e	0.67	0.66	0.73	0.68	0.68	0.67
Hokkaido	m/s^2	15.23	10.09	9.94	10.60	10.11	10.12	9.96
	Ratio	e	0.66	0.65	0.70	0.66	0.66	0.65
Average Reduction Ratio			0.65	0.64	0.68	0.64	0.66	0.66

within the seismic response reduction rate of the existing TMD optimum design values. The dynamic interpretation of the

Table 11
Comparison of RMS acceleration responses.

Earthquake ground motions	Unit	w/o TMD	w/TMD					
			Den Hartog	Warburton	Sadek et al.	Rana & Soong	Kwag et al.	Actual TMD
OPR FRS	m/s^2	1.77	0.99	0.99	1.05	1.00	0.99	0.99
	Ratio	e	0.56	0.56	0.59	0.56	0.56	0.56
DGRS	m/s^2	3.81	2.53	2.54	2.59	2.52	2.53	2.56
	Ratio	e	0.66	0.67	0.68	0.66	0.67	0.67
El Centro	m/s^2	1.76	1.08	1.08	1.14	1.08	1.08	1.08
	Ratio	e	0.61	0.61	0.65	0.62	0.61	0.61
Hokkaido	m/s^2	3.91	1.97	2.00	2.04	2.00	1.96	1.96
	Ratio	e	0.51	0.51	0.52	0.51	0.50	0.50
Average Reduction Ratio			0.59	0.59	0.61	0.59	0.59	0.59

Table 12
Comparison of maximum spectral acceleration responses.

Earthquake ground motions	Unit	w/o TMD	w/TMD					
			Den Hartog	Warburton	Sadek et al.	Rana & Soong	Kwag et al.	Actual TMD
OPR FRS	m/s^2	37.76	15.74	15.65	18.62	16.53	15.47	14.77
	Ratio	e	0.42	0.41	0.49	0.44	0.41	0.39
DGRS	m/s^2	66.54	35.25	35.81	41.39	36.31	35.71	35.55
	Ratio	e	0.53	0.54	0.62	0.55	0.54	0.53
El Centro	m/s^2	44.52	24.37	23.86	28.53	24.63	24.45	23.56
	Ratio	e	0.55	0.54	0.64	0.55	0.55	0.53
Hokkaido	m/s^2	120.45	36.07	36.56	43.91	38.83	34.88	31.70
	Ratio	e	0.30	0.30	0.36	0.32	0.29	0.26
Average Reduction Ratio			0.45	0.45	0.53	0.47	0.45	0.43

developed TMD and actual nuclear piping will help understand and practice such experiments in the future. For a complete study, additional shaking table studies are required to analyze the combined model of actual piping and the TMD.

Declaration of competing interest

The authors declare that they have no known competing financial interests or personal relationships that could have appeared to influence the work reported in this paper.

Acknowledgments

This study was supported by the Ministry of Trade, Industry and Energy through KETEP (Korea Institute of Energy Technology Evaluation Planning) (No. 20181510102380). The first author appreciates the financial support of the National Research Foundation of Korea (NRF) grant funded by the Korea government (Ministry of Science and ICT) (No. 2020R1G1A1005510).

References

[1] S. Kwag, D. Hahm, Development of an earthquake-induced landslide risk assessment approach for nuclear power plants, Nucl. Eng. Technol. 50 (8) (2018) 1372e1386.
[2] S. Kwag, Y. Ryu, B.S. Ju, Efficient seismic fragility analysis for large-scale piping system utilizing Bayesian approach, Appl. Sci. 10 (4) (2020) 1515.
[3] S. Kwag, A. Gupta, Probabilistic risk assessment framework for structural systems under multiple hazards using Bayesian statistics, Nucl. Eng. Des. 315 (2017) 20e34.
[4] B.S. Ju, S.K. Tadinada, A. Gupta, Fragility analysis of threaded T-joint connections in hospital piping systems, in: Pressure Vessels and Piping Conference, vol. 44588, 2011, January, pp. 147e155.
[5] Y. Tian, Experimental Seismic Study of Pressurized Fire Sprinkler Piping Subsystems, State University of New York at Buffalo, 2013.
[6] D. Hahm, J. Park, I.K. Choi, Seismic performance evaluation of piping system crossing the isolation interface in seismically isolated NPP, J. Earthq. Eng. Soc. Korea 18 (3) (2014) 141e150.
[7] Y. Tian, A. Filiatrault, G. Mosqueda, Seismic response of pressurized fire sprinkler piping systems I: experimental study, J. Earthq. Eng. 19 (4) (2015) 649e673.
[8] Y. Tian, A. Filiatrault, G. Mosqueda, Seismic response of pressurized fire sprinkler piping systems II: numerical study, J. Earthq. Eng. 19 (4) (2015b) 674e699.
[9] B.G. Jeon, S.W. Kim, H.S. Choi, D.U. Park, N.S. Kim, A failure estimation method of steel pipe elbows under in-plane cyclic loading, Nucl. Eng. Technol. 49 (1) (2017) 245e253.
[10] S.W. Kim, H.S. Choi, B.G. Jeon, D.G. Hahm, Low-cycle fatigue behaviors of the elbow in a nuclear power plant piping system using the moment and deformation angle, Eng. Fail. Anal. 96 (2019) 348e361.
[11] B.S. Ju, W.Y. Jung, Y.H. Ryu, Seismic fragility evaluation of piping system installed in critical structures, Struct. Eng. Mech. 46 (3) (2013) 337e352.
[12] B.S. Ju, A. Gupta, Seismic fragility of threaded Tee-joint connections in piping systems, Int. J. Pres. Ves. Pip. 132 (2015) 106e118.
[13] S. Soroushian, A.E. Zaghi, M. Maragakis, A. Echevarria, Y. Tian, A. Filiatrault, Analytical seismic fragility analyses of fire sprinkler piping systems with threaded joints, Earthq. Spectra 31 (2) (2015) 1125e1155.
[14] M. Kunieda, T. Chiba, H. Kobayashi, Positive use of damping devices for piping systems d some experiences and new proposals, Nucl. Eng. Des. 104 (2) (1987) 107e120.
[15] Y. Park, G. DeGrassi, C. Hofmayer, P. Bezler, N. Chokshi, Analysis of Nuclear Piping System Seismic Tests with Conventional and Energy Absorbing Supports (No. BNL-NUREG-64173; CONF-970826-7), Brookhaven National Lab., Upton, NY (United States), 1997.
[16] K. Fujita, T. Kimura, Y. Ohe, Seismic response analysis of piping systems with nonlinear supports using differential algebraic equations, J. Pressure Vessel Technol. 126 (1) (2004) 91e97.
[17] S.V. Bakre, R.S. Jangid, G.R. Reddy, Seismic response of piping systems with isolation devices, in: Proceedings of the 13th World Conference on Earthquake Engineering, 2004, August.
[18] S.V. Bakre, R.S. Jangid, G.R. Reddy, Optimum X-plate dampers for seismic response control of piping systems, Int. J. Pres. Ves. Pip. 83 (9) (2006) 672e685.
[19] P. Kumar, R.S. Jangid, G.R. Reddy, Response of piping system with semi-active variable stiffness damper under tri-directional seismic excitation, Nucl. Eng. Des. 258 (2013) 130e143.
[20] P. Kumar, R.S. Jangid, G.R. Reddy, Comparative performance of passive devices for piping system under seismic excitation, Nucl. Eng. Des. 298 (2016) 121e134.
[21] S. Rechenberger, D. Mair, Vibration control of piping systems and structures using tuned mass dampers, in: ASME 2017 Pressure Vessels and Piping Conference (Pp. V03BT03A035-V03BT03A035), American Society of Mechanical Engineers, 2017, July.
[22] G.B. Song, P. Zhang, L.Y. Li, M. Singla, D. Patil, H.N. Li, Y.L. Mo, Vibration control of a pipeline structure using pounding tuned mass damper, J. Eng. Mech. 142 (6) (2016), 04016031.
[23] J. Jiang, P. Zhang, D. Patil, H.N. Li, G. Song, Experimental studies on the

effectiveness and robustness of a pounding tuned mass damper for vibration suppression of a submerged cylindrical pipe, Struct. Contr. Health Monit. 24 (12) (2017), e2027.
[24] W. Wang, D. Dalton, X. Hua, X. Wang, Z. Chen, G. Song, Experimental study on vibration control of a submerged pipeline model by eddy current tuned mass damper, Appl. Sci. 7 (10) (2017) 987.
[25] J. Tan, M. Ho, S. Chun, P. Zhang, J. Jiang, Experimental study on vibration control of suspended piping system by single-sided pounding tuned mass damper, Appl. Sci. 9 (2) (2019) 285.
[26] S. Kwag, J. Kwak, H. Lee, J. Oh, G.H. Koo, Enhancement in the seismic performance of a nuclear piping system using multiple tuned mass dampers, Energies 12 (11) (2019) 2077.
[27] H. Frahm, Device for Damping Vibrations of Bodies, 1909. U.S. Patent No.989958.
[28] K.C.S. Kwok, B. Samali, Performance of tuned mass dampers under wind loads, Eng. Struct. 17 (9) (1995) 655e667.
[29] T.T. Soong, G.F. Dargush, Passive Energy Dissipation Systems in Structural Engineering, John Wiley & Sons Ltd., Chichester, England, 1997.
[30] S. Chang, W. Sun, S.G. Cho, D. Kim, Vibration control of nuclear power plant piping system using stockbridge damper under earthquakes, Sci. Technol. Nucl. Instal. (2016) 12, 2016, Article ID 5014093.
[31] B. Li, K. Dai, H. Li, B. Li, S. Tesfamariam, Optimum design of a non-conventional multiple tuned mass damper for a complex power plant structure, Struct. Infrastruct. Eng. 15 (7) (2019) 954e964.
[32] S.G. Cho, S. Chang, D. Sung, Application of tuned mass damper to mitigation of the seismic responses of electrical equipment in nuclear power plants, Energies 13 (2) (2020) 427.
[33] M. Khazaee, S.E. Khadem, A. Moslemi, A. Abdollahi, Vibration mitigation of a pipe conveying fluid with a passive geometrically nonlinear absorber: a tuning optimal design, Commun. Nonlinear Sci. Numer. Simulat. 91 (2020) 105439.
[34] Kaeri, Ultimate-level Seismic Performance Evaluation of a Piping System. KAERI/CM-1402/2010, Korea Atomic Energy Research Institute, Daejeon, Korea, 2010.
[35] J.P. Den Hartog, Mechanical Vibrations, MaGraw-Hill, 1956, p. 87, 1956.
[36] G.B. Warburton, Optimum absorber parameters for various combinations of response and excitation parameters, Earthq. Eng. Struct. Dynam. 10 (3) (1982) 381e401.
[37] F. Sadek, B. Mohraz, A.W. Taylor, R.M. Chung, A method of estimating the parameters of tuned mass dampers for seismic applications, Earthq. Eng. Struct. Dynam. 26 (6) (1997) 617e635.
[38] R. Rana, T.T. Soong, Parametric study and simplified design of tuned mass dampers, Eng. Struct. 20 (3) (1998) 193e204.
[39] V.B. Bhandari, Design of Machine Elements, Tata McGraw-Hill Education, 2010.
[40] A.K. Chopra, Dynamics of Structures, Pearson Education, Upper Saddle River, NJ, 2012.
[41] S. Kwag, J. Park, I.K. Choi, Development of efficient complete-sampling-based seismic PSA method for nuclear power plant, Reliab. Eng. Syst. Saf. 197 (2020b) 106824.
[42] S.W. Kim, B.G. Jeon, D.G. Hahm, M.K. Kim, Seismic fragility evaluation of the base-isolated nuclear power plant piping system using the failure criterion based on stress-strain, Nucl. Eng. Technol. 51 (2) (2019) 561e572.
[43] S. Kwag, J. Kwak, H. Lee, J. Oh, G.H. Koo, A numerical study on improvement in seismic performance of nuclear components by applying dynamic absorber, J. Comput. Struct. Eng. Inst. Korea 32 (1) (2019b) 17e27.
[44] USNRC RG 1.60, Rev. 2, Design Response Spectra for Seismic Design of Nuclear Power Plants.